Experimental results of a modified condensation-driven dilution refrigerator by adding a step heat exchanger

Weijun Cheng[1,2], Hongye Zu[3], Zhiheng Li[1,2], Yanan Wang[1*], Wei Dai[1,2]

[1] Key Laboratory of Cryogenic Science and Technology, Technical Institute of Physics and Chemistry, Chinese Academy of Sciences, Beijing 100190, China

[2] University of Chinese Academy of Sciences, Beijing 100049, China

[3] BYD Automobile Industry Co., Ltd, Shenzhen 518000, China

[*]E-mail: wangyanan@mail.ipc.ac.cn

Abstract. Condensation-driven dilution refrigerator uses a condenser to liquefy the ^{3}He vapor and achieve the circulation of the ^{3}He, which can meet the requirements of specific applications, such as the forthcoming generation of cosmic microwave background observatories. In 2023, we built a condensation-driven dilution refrigerator with a no-load temperature of 68 mK, and the cooling performance needs further improvement. In this paper, the condensation-driven dilution refrigerator is modified, and a step heat exchanger with sintered silver powder is added to the system. The step heat exchanger with a total surface area of 3 m^2 is designed to efficiently meet the heat transfer requirements. In the experiments, the no-load temperature of 55.3 mK and a cooling power of 7.4 μW @100 mK were achieved in the modified system.

Keywords: Sub-kelvin, Dilution refrigerator, Condensation, Step heat exchanger, Kapitza resistance

1. Introduction

Dilution refrigerator (DR) is extensively used in condensed matter physics research, quantum devices, and astronomical observations [1]. According to the types of circulating pumps, DRs can be divided into conventional DRs using mechanical pumps and cold-cycle DRs with cryogenic adsorption pumps or condensation pumps [2].

Conventional DRs need complex external gas circulation systems that produce mechanical vibrations that ought to be suppressed [3]. The condensation-driven dilution refrigerator (CDR) employs a condensation pump to achieve the circulation of ^{3}He, having advantages such as a compact structure, lightweight, low cost, and reduced vibration [4]. With these characteristics, the CDR can meet the requirements of specific applications requiring a compact and easy-to-operate cryocooler for detector cooling [4], [5].

The CDR was first proposed by V. S. Edel'man et al. [6] in 1972. Early CDR with the 1 K liquid helium bath can achieve a minimum temperature of 12.1 mK [7]. The advances in 4 K GM

cryocoolers led to the development of cryogen-free CDR (or dry CDR), which has now become mainstream. The lowest temperature achieved is 48 mK [4] and generally provides μW-class cooling power at 100 mK [8]. In 2024, we built a CDR with the no-load temperature of 68 mK [9], and the performance needs further improvement. The following introduces our most recent work by adding a step heat exchanger to the system.

2. Refrigeration principle and experimental setup of CDR

The DR uses the properties of a ^{3}He-^{4}He mixture for cooling. The cooling power of the Mixing Chamber (MC) equals the enthalpy difference between the incoming and outgoing fluids [1]:

$$Q_{mc} = n_3(H_{3,d}(x_s, T_{mc}) - H_3(T_i)) \quad (1)$$

In the equation (1), n_3 (mol/s) represents the flow rate of ^{3}He, $H_{3,d}$ and H_3 (J/mol) denote the enthalpy of one mole of ^{3}He in the dilute and concentrated phases respectively, T_{mc} (K) is the temperature of MC, x_s is the saturation concentration corresponding to T_{mc}, and T_i (K) is the inlet temperature of the MC.

Figure 1 illustrates the schematic of the CDR and the corresponding setup in our lab is shown in Figure 2. The CDR consists of a condensation pump (CP), heat exchanger (HEX), MC, and still. The experiment uses a GM-type pulse tube cryocooler (SRP-082B) from Sumitomo Heavy Industries to provide the pre-cooling at 4 K and a two-stage adsorption refrigerator (AR) GL-7 from Chase Research Cryogenics to provide the 1 K and 0.4 K heat sink required by the CDR.

Heat transfer between the CP and the ^{3}He cold head (AR cold plate) is facilitated by a thermal link. Passive superconducting thermal switches (lead wire) are positioned between the MC and

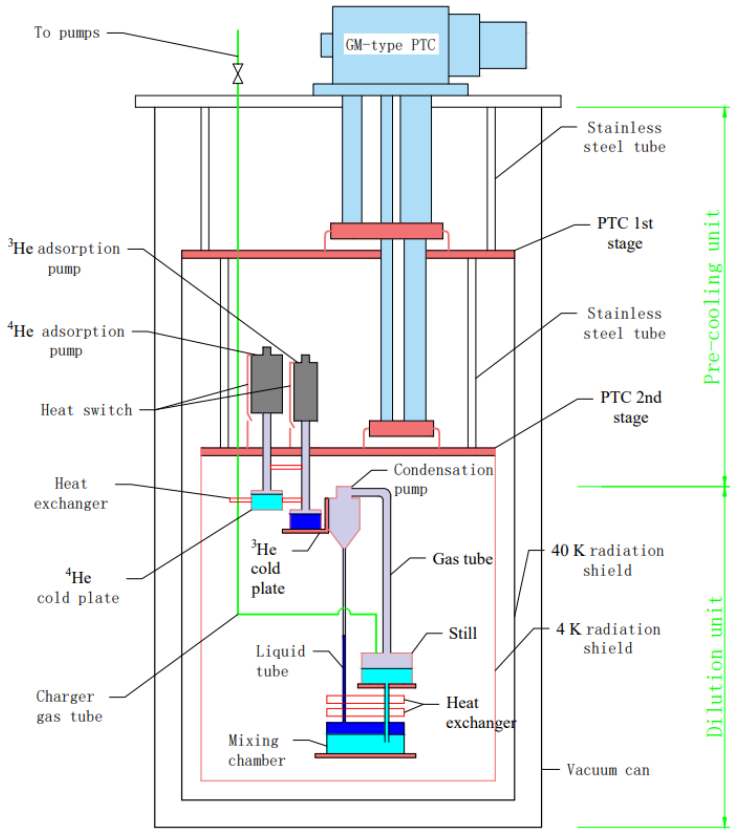

Figure 1. The schematic of the CDR.

the ^{3}He cold head, while an active gap thermal switch is placed between the still and the ^{4}He cold head to enhance the cool-down speed from ambient temperature.

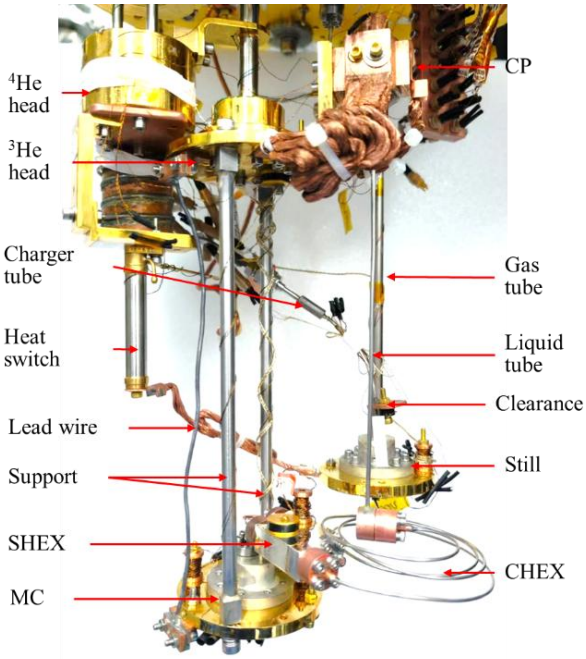

Figure 2. The experimental setup of CDR.

The achievable lowest temperature and cooling power of CDR are closely related to the temperature of the concentrated phase entering the MC, which is primarily determined by the performance of the counterflow HEX. The HEX must feature a sufficient heat transfer area while keeping axial thermal conduction and viscous dissipation to a minimum value relative to the heat transfer rate. An annular clearance with a hydraulic diameter of tens of micrometers was arranged in the connection between the still and charger tube to inhibit the superfluid creep.

In summary, the CHEX adopts a tube-in-tube configuration, utilizing $Cu_{70}Ni_{30}$ tube with a length of 800 mm. The outer diameter of the dilute phase and concentrated phase tubing is 1.4 mm and 0.6 mm respectively, with a wall thickness of 0.1 mm. The step heat exchanger (SHEX) with sintered silver powder is illustrated in Figure 3. The SHEX is constructed using silver powder with a particle size of 200 nm, the same material utilized on the bottom of the MC. To reduce viscous heating, small empty flow passages are prepared in the middle of the channels and surrounded by the sintered silver sponge. The specific surface area of sintered silver powder is measured to be 1 m^2/g by Brunauer– Emmett–Teller (BET) adsorption isotherm.

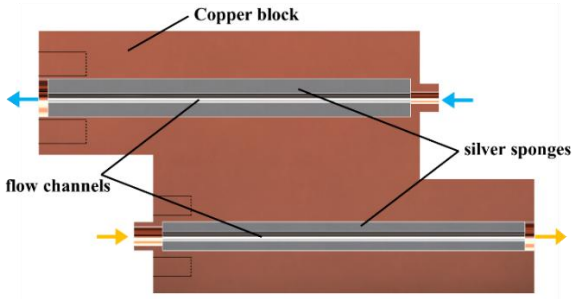

Figure 3. Schematic of a step heat exchanger made from Cu block into which two flow channels for the counter-flowing liquids have been prepared, sintered silver powder on the channel wall.

3. Experiment results and discussion

The system is charged with 5.2 liters of the ^{3}He-^{4}He mixture, characterized by a 24% concentration of ^{3}He, corresponding to a phase separation temperature of 500 mK. The cooling time from room temperature to 4 K takes approximately 30 hours. Subsequently, the ^{4}He stage of the AR is cooled to a temperature below Sub-K.

Figure 4 shows the temperature curves starting from about 0.9 K. The heating of the still keeps being adjusted to maintain its temperature above 0.7 K. With a heating power of 320 μW for the still, a no-load temperature of 57.5 mK is achieved. A thermometer ($T_{\text{clearance}}$) was placed near the clearance to help diagnose the superfluid creep or the gas flow to the charger tube. Another special thermometer ($T_{\text{cp, inlet}}$) was placed on the outside of the gas tube near the condensation pump.

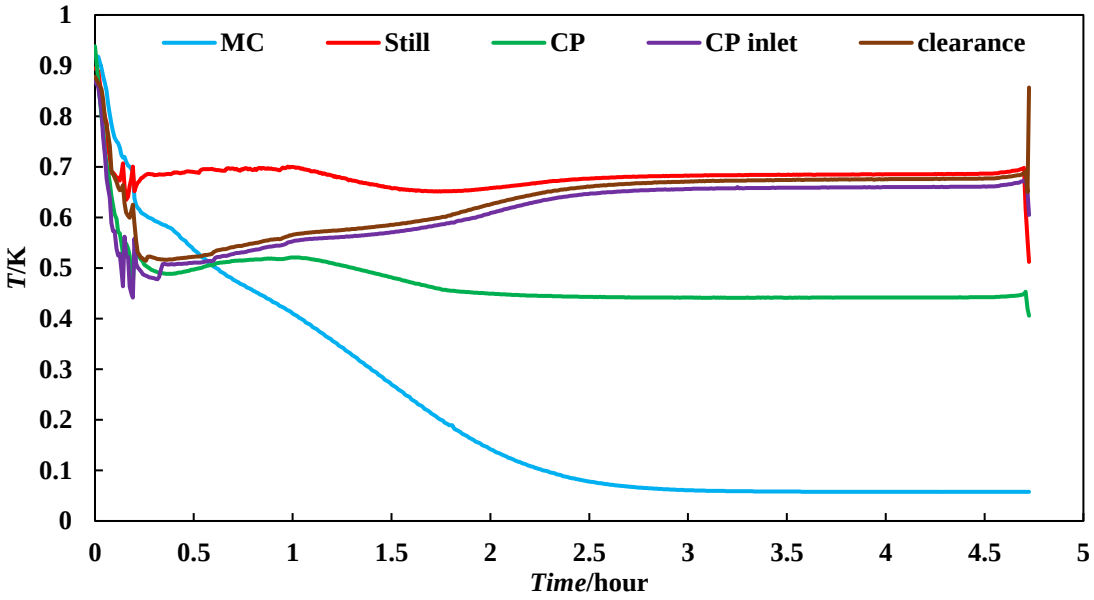

Figure 4. Temperature curve of the no-load temperature experiment of CDR.

The relationship between the lowest temperature at the MC and the heating power of the still (Q_s) is shown in Figure 5 (a). When the Q_s exceeds 400 μW, the no-load T_{mc} drops below 56 mK. Further increasing the Q_s just results in a small change in the no-load T_{mc}. The reason for this is that an increase in Q_s results in a rise in the temperature in the still (T_s), which leads to a bigger amount of evaporated ^{4}He from the still. The evaporated ^{4}He unnecessarily consumes part of the cooling power provided by the CP, and more importantly, reduces the heat transfer efficiency of the HEX. As a result, although the system circulation flow rate increases, the change in the no-load T_{mc} is not significant.

As shown in Figure 5 (b), the system performance using both CHEX and SHEX is not always superior to that using only CHEX. At a lower T_{mc}, under the same still heating power, the system with CHEX and SHEX can achieve greater cooling power. However, at a higher T_{mc}, the system with CHEX performs better. The transition point for the system studied here is approximately 120 mK.

With a decrease in the T_{mc}, the influence of Kapitza resistance becomes more pronounced, leading to a degradation in the CHEX performance. Conversely, the SHEX demonstrates its ability to lower the Kapitza resistance. Despite operating with a smaller circulation flow rate in the CHEX + SHEX system, the enhanced heat transfer efficiency allows for the achievement of higher cooling power.

The relationship between the cooling power of the MC (Q_{mc}) at 100 mK and the Q_s is shown in Figure 7. When the Q_s is low, the Q_{mc} exhibits a linear relationship with the Q_s. As the Q_s exceeds

400 μW, the Q_{mc} reaches 5.2 μW. With the further increase in heating power, the impact on Q_{mc} becomes less remarkable. At a Q_s of 700 μW, the Q_{mc} is 7.4 μW. The possible reason is that, as Q_s increase, both the T_s and the temperature of CP (T_{cp}) rise, leading to an increase in the amount of evaporated ^{4}He from the still. The T_{cp} also increases, which leads to a warmer condensed liquid. Both have a negative influence on the system's performance.

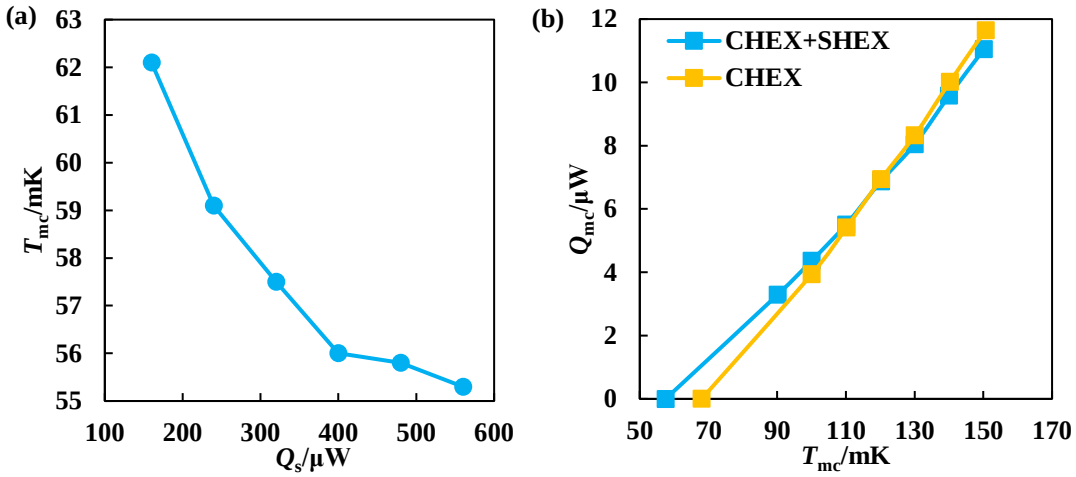

Figure 5. Experimental results at different MC temperatures: (a) the lowest temperature; (b) cooling power.

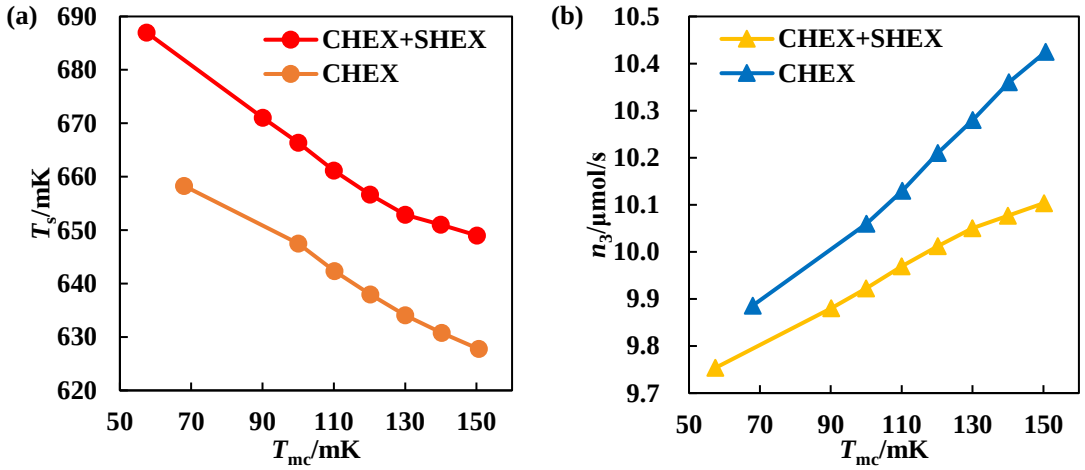

Figure 6. Calculation results at different MC temperatures: (a) the still temperature; and (b) the ^{3}He circulation flow rate.

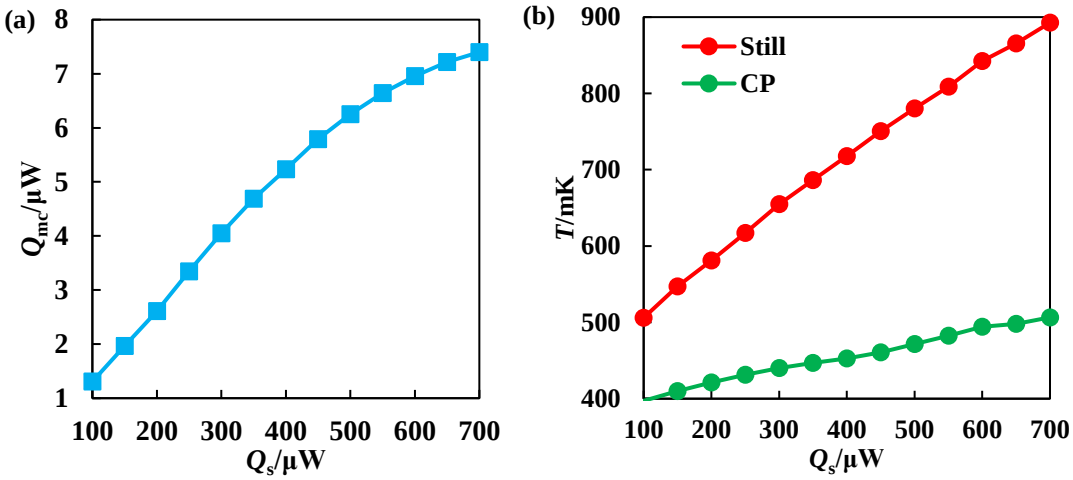

Figure 7. Dependence of Q_{mc} at 100 mK (a) and corresponding T_{cp} and T_{still} (b).

4. Conclusion

In this paper, experimental results of a modified condensation-driven dilution refrigerator were reported. We have developed a CDR with a continuous heat exchanger and step heat exchanger using sintered silver powder, which achieves a no-load temperature of 55.3 mK, and a cooling power of 7.4 μW at 100 mK. Compared with previous experiments, using a step heat exchanger is effective in obtaining a lower cooling temperature. The influence of key parameters on the system performance has also been investigated and possible reasons are given.

Acknowledgment. This work is financially supported by the National Natural Science Foundation of China (Grant No. 52176027). We thank A.T.A.M. de Waele for the valuable discussions.

References

[1] Pobell, F. (2007). Matter and Methods at Low Temperatures. Berlin, Heidelberg Springer Berlin Heidelberg.
[2] Zu, H., Dai, W. and de Waele, A.T.A.M. (2021). Development of dilution refrigerators—A review. Cryogenics, p.103390. doi:https://doi.org/10.1016/j.cryogenics.2021.103390.
[3] Hata, T., Matsumoto, T., Obara, K., Yano, H., Ishikawa, O., Handa, A., Togitani, S. and Nishitani, T. (2013). Development and Comparison of Two Types of Cryogen-Free Dilution Refrigerator. Journal of Low Temperature Physics, 175(1-2), pp.471–479. doi:https://doi.org/10.1007/s10909-013-0986-3.
[4] Gustav Teleberg, Chase, S.T. and Piccirillo, L. (2006). A miniature dilution refrigerator for sub-Kelvin detector arrays. Proceedings of SPIE, the International Society for Optical Engineering/Proceedings of SPIE, 6275, pp.62750D62750D. doi:https://doi.org/10.1117/12.671851.
[5] May, A.J., Calisse, P.G., Coppi, G., Haynes, V., Martinis, L., McCulloch, M.A., Melhuish, S.J. and Piccirillo, L. (2016). Sorption-cooled continuous miniature dilution refrigeration for astrophysical applications. Proceedings of SPIE, the International Society for Optical Engineering/Proceedings of SPIE. doi:https://doi.org/10.1117/12.2232609.
[6] V.S. Edel'man (1972). A dilution refrigerator with condensation pump. Cryogenics, 12(5), pp.385–387. doi:https://doi.org/10.1016/0011-2275(72)90114-2.
[7] V.E. Sivokon, V.V. Dotsenko, L.A. Pogorelov and Sobolev, V.I. (1992). Dilution refrigerator with condensation pumping. Cryogenics, 32, pp.207–210. doi:https://doi.org/10.1016/0011-2275(92)90144-y.
[8] Chase, S.T., Brien, T.L.R., Doyle, S.M. and Kenny, L.C. (2019). Pre-cooling a 3He/4He dilutor module with a sealed closed-cycle continuous cooler. IOP Conference Series: Materials Science and Engineering, 502, p.012134. doi:https://doi.org/10.1088/1757-899x/502/1/012134.
[9] Cheng, W., Zu, H., Li, Z., Wang, Y. and Dai, W. (2024). Thermodynamic analysis and optimization of a condensation-driven dilution refrigerator. Journal of Applied Physics, 135(23). doi:https://doi.org/10.1063/5.0203218.